Recycled PET Nanocomposites Improved by Silanization of Organoclays

Milan Kráčalík,[1] Martin Studenovský,[2] Jana Mikešová,[2] Antonín Sikora,[2,3] Ralf Thomann,[4] Christian Friedrich,[4] Ivan Fortelný,[2,3] Josef Šimoník[3†]

[1]*Institute of Plastics Processing, University of Leoben, 8700 Leoben, Austria*
[2]*Institute of Macromolecular Chemistry, Academy of Sciences of the Czech Republic, 162 06 Prague 6, Czech Republic*
[3]*Faculty of Technology, Tomas Bata University in Zlín, 762 72 Zlín, Czech Republic*
[4]*Freiburg Materials Research Center, University of Freiburg, 79104 Freiburg, Germany*

Received 6 April 2006; accepted 12 March 2007
DOI 10.1002/app.26690
Published online 3 July 2007 in Wiley InterScience (www.interscience.wiley.com).

ABSTRACT: Recycled PET/organo-modified montmorillonite nanocomposites were prepared via melt compounding as a promising possibility of the used beverage bottles recovery. According to our previous work, the three suitable commercial organoclays Cloisite 25A, 10A, and 30B were additionally modified with [3-(glycidyloxy)propyl]trimethoxysilane, hexadecyltrimethoxysilane and (3-aminopropyl)trimethoxysilane. The selected organoclays were compounded in the concentration 5 wt % and their degree of intercalation/delamination was determined by wide-angle X-ray scattering and transmission electron microscopy. Modification of Cloisite 25A with [3-(glycidyloxy)-propyl]trimethoxysilane increased homogeneity of silicate layers in recycled PET. Additional modification of Cloisite 10A and Cloisite 30B led to lower level of delamination concomitant with melt viscosity reduction. However, flow characteristics of all studied organoclay nanocomposites showed solid-like behavior at low frequencies. Silanization of commercial organoclays had remarkable impact on crystallinity and melt temperature decrease accompanied by faster formation of crystalline nuclei during injection molding. Thermogravimetric analysis showed enhancement of thermal stability of modified organoclays. The tensile tests confirmed significant increase of PET-R stiffness with organoclays loading and the system containing Cloisite 25A treated with [3-(glycidyloxy)propyl]trimethoxysilane revealed combination of high stiffness and extensibility, which could be utilized for production of high-performance materials by spinning, extrusion, and blow molding technologies. J Appl Polym Sci 106: 926–937, 2007

Key words: recycled PET; organoclay; silanization

INTRODUCTION

Poly(ethylene)terephthalate (PET) is a semicrystalline polymer with high chemical resistance, thermal stability, melt mobility, spinnability, and low permeability to gases. Applications of PET are directed to different industrial branches, such as packaging, textile, automotive, electro-technical, construction, and other industries.[1–3] Industrial production of PET bottles started in the USA in the 80s, using advantageous properties of PET, such as low weight, high impact resistance, nontoxic nature, and high transparency.[4] Due to the growing amount of PET used in plastics industry (especially for beverage bottles), finding various proper methods of recycling is an emergent challenge from the ecological and economical points of view.[5] The amount of recycled PET bottles in PET-reprocessing countries is usually only 20–30 wt %. The rest of the used bottles ends in energy recovery or in deposits.[6]

At present, two PET recovery methods are used: chemical and physical recycling. Chemical depolymerization[7] is economical only for high amounts of waste. On the other hand, physical (mechanical, material) recycling is a convenient way for economical and environmental purposes.[6,8,9] Some high-tech pilot projects with recycled PET bottles have been tested[4,5,10,11]; nevertheless, PET staple fibers with limited application still occupy the market. In particular, no study of PET recovery for the purpose of nanocomposite materials with improved processing and utility properties has been found in available literature.

In our previous work, the viscosity decrease of recycled PET during processing was investigated.[12] The study showed that reprocessing of PET waste with the intrinsic viscosity value below 0.7 dL/g is

Correspondence to: M. Kráčalík (Milan.Kracalik@mu leoben.at).

Contract grant sponsor: Ministry of Environment of the Czech Republic; contract grant number: VaV-1C/7/48/04.
Contract grant sponsor: Academy of Sciences of the Czech Republic; contract grant number: AVOZ 40500505.

† Diseased.

not possible.[6] However, viscosity of the recycled polymer can be increased by filler addition. In the effort not to deteriorate mechanical properties of the material, nanofillers seem interesting.

Nanotechnology was introduced as a new method of improvement of polymer properties in 1995. The technology involves not only incorporation of nanosized particles into the polymer but, more importantly, investigation of interactions between the polymer matrix and the enormously large nanofiller surface.[13] Especially for polymer/clay nanocomposites, the surface effects are responsible for improvement of barrier, mechanical and rheological properties, dimensional stability, heat, flame, and oxidative resistance. In comparison with traditional fillers (20−40 wt % loading), 2−5 wt % filling of layered clays is sufficient to achieve analogous material improvement.[14,15] Generally, three methods of the polymer/clay nanocomposites preparation are used: *in situ* polymerization, solution mixing, and melt mixing.[16,17] In the case of PET/clay systems, the first two techniques were successfully tested.[18–28] The melt mixing process is technologically much more interesting; nevertheless, satisfactory results with PET have not been achieved.[29,30,31]

Despite sensitivity of melt rheology to changes in structure of the dispersed nanoparticles in the matrix, rheological experiments have been so far rarely used in investigation and characterization of polymer nanocomposites. A few rheological studies of polymer/clay systems, usually concerning nanocomposites with polyamides, confirm the enormous viscosity increase associated with clay loading in the region of low shear rates. The connection between the level of delamination of silicate platelets and formation of a physical network, indicated by secondary G' and G'' plateaus,[13,30–45] was also published. For the PET/clay systems, Sanchez-Solis et al.[30,31] reported the reduction of the shear viscosity and storage modulus explained by a decrease in particle–matrix interactions.

According to our work, addition of organoclays to recycled PET led to transparent nanocomposites with enhanced rheological, thermal, and mechanical properties. For the extrusion technology, the loss of melt strength causes an incohesion of material after leaving the extrusion die and, consequently, makes impossible the production of sheets or precise profiles. On the other hand, injection molding requires sufficient flow of polymer melts, which is carried out by alignment of silicate platelets in the flow direction at a high shear rates. Therefore, both processing technologies can be applied to recycled PET nanocomposites production. Possible applications of the recycled polymer/clay systems could be found in various industry fields, which would utilize enhancement of strength, thermal, barrier, and other material properties, such as in car components (combination of barrier and strength characteristics), building industry, etc.

Our previous results confirmed improvement of processing properties by addition of commercial organoclays to recycled PET. Nevertheless, moderate degrading reactions were detected during the mixing in micro-extruder.[46] With a view to reduce the mentioned degradation and to increase delamination in the system, the selected commercial organoclays were additionally modified. The principle of the treatment consists in silanization of clay hydroxy groups by the selected silanes in aqueous-methanolic environment. The bonded functional groups can facilitate chemical or physical interaction of the filler with the polymer matrix and eliminate the degrading nature of the silicate hydroxyl groups (hydrolysis of PET).

The aim of the study was to investigate effects of additionally modified organoclays on rheological properties of recycled PET with the goal to enhance PET bottles recovery and to test utility properties of the prepared nanocomposites.

EXPERIMENTAL

Materials

The commercial organoclays were produced by Southern Clay Products, Gonzales, TX. The specifications of the organoclays are summarized in Table I. Nine new organoclays were prepared by additional modification (Fig. 1, Table II).

Color-sorted recycled poly(ethylene)terephthalate (PET-R), with the intrinsic viscosity 0.73 dL/g (dilution in phenol/tetrachloroethane 1 : 3), supplied by Polymer Institute Brno, was used as matrix. As can be seen in Figure 2, PET-R exhibits usual thermal behavior (similar to virgin bottle grade PET) because no remarkable decrease in T_g (T_m) magnitude occurred.

TABLE I
Specification of Commercial Organoclays[a]

Organoclay	Organic modifier[b]	Modifier concentration (mequiv/ 100 g clay)	Moisture (%)	Weight loss on ignition (%)
Cloisite 25A	2MHTL8	95	<2	34
Cloisite 10A	2MBHT	125	<2	39
Cloisite 30B	MT2EtOH	90	<2	30

[a] According to the manufacturer.
[b] Quaternary ammonium chlorides: alkyl(2-ethylhexyl)-dimethyl (2MHTL8), alkyl(benzyl)dimethyl (2MBHT), alkylbis(2-hydroxyethyl)methyl (MT2EtOH). Alkyls are a mixture of 65% C18, 30% C16, and 5% C14, derived from hydrogenated tallow.

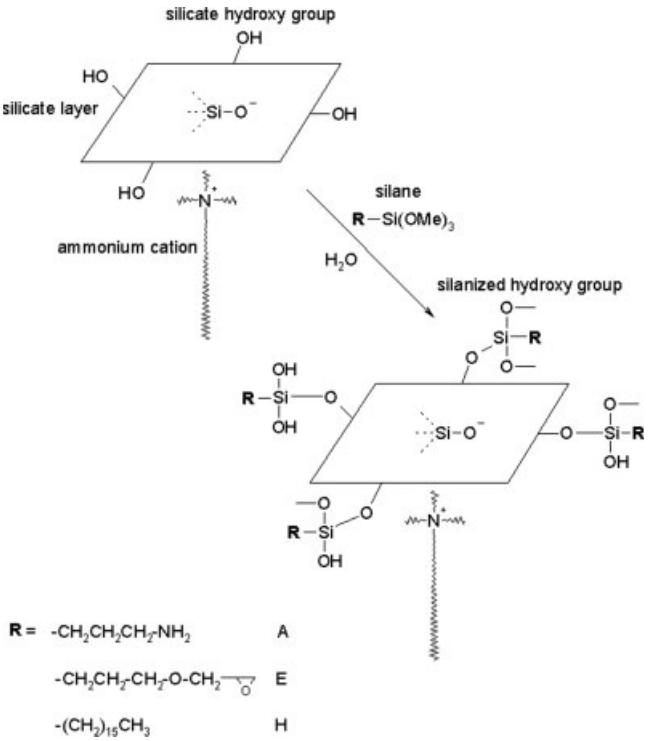

Figure 1 Chemical modification of commercial organoclays.

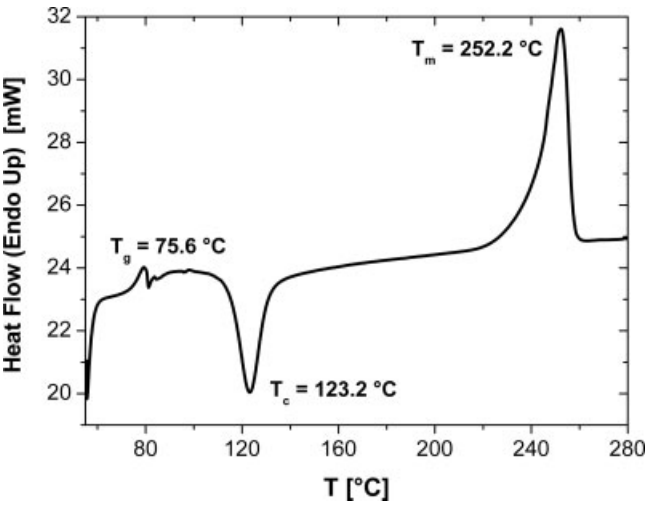

Figure 2 DSC thermograph of the recycled PET matrix.

Preparation of silanized organoclays

The commercial organoclay (1 g) was suspended in 50 mL of methanol–water mixture (10 : 1) with subsequent addition of silane (0.3 g). The mixture was stirred for 2 days at room temperature and the precipitate was filtered off and rigorously washed with methanol. The solid was dried under vacuum at 50°C for 4 h.

Preparation of recycled PET/organoclay nanocomposites

Organically modified clays (om-MMT) were dried at 80°C and PET regranulated at 110°C in oven at least for 12 h. The recycled polymer was mixed with 5 wt % (relative to the anorganic part of organoclays) of om-MMT in a corotating twin-screw micro-extruder (DSM Research, Netherlands) under nitrogen atmosphere. The compounding temperature was 255°C to exert maximal shear stress and minimal thermal degradation on the modified montmorillonite during processing. The mixing time of PET granules and organoclay powder was 10 min at the speed 200 rpm. The time dependences of load force were measured in the micro-extruder during mixing. Recycled PET nanocomposites were injection-molded (micro-injection system; DSM Research) to specimens for mechanical, rheological, thermal, and wide-angle X-ray scattering (WAXS) testing at 260–265°C. The duration of injection cycle was ca. 10 s. The samples for TEM measurements were vacuum-compression molded at 260°C for 5 min (hydraulic laboratory plate press machine Collin 200P) due to higher isotropy of silicate platelets in polymer matrix.

TABLE II
Indication of Silanized Organoclays

	Modifier/prepared organoclay		
Commercial organoclay	E[a]	H[b]	A[c]
Cloisite 25A	C 25AE	C 25AH	C 25AA
Cloisite 10A	C 10AE	C 10AH	C 10AA
Cloisite 30B	C 30BE	C 30BH	C 30BA

[a] [3-(glycidyloxy)propyl]trimethoxysilane.
[b] Hexadecyltrimethoxysilane.
[c] (3-Aminopropyl)trimethoxysilane.

Melt rheology

Rheological properties were studied using an ARES 3 Rheometer (Advanced Rheometric Expanded System; Rheometric Scientific, Piscataway, NJ) with a parallel-plate geometry of 25-mm-diameter plates. All measurements were performed with two automatically switched force transducers with a torque range of 0.02−2000 g cm. The samples thickness ranged from 0.9 to 1.1 mm. Experiments were performed at 270°C under nitrogen (liquid N_2 source) to prevent degradation of samples. The following types of rheological measurements were carried out: (1) dynamic strain sweep test (at 6.28 rad/s) to confirm the linearity of viscoelastic region, (2) dynamic frequency sweep test over a frequency range of

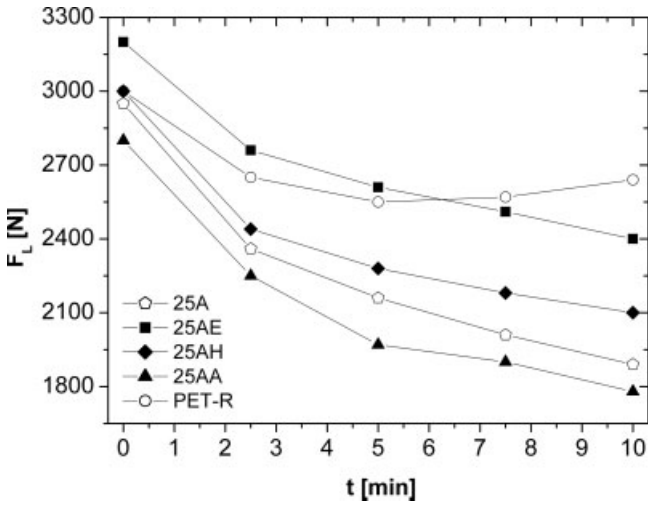

Figure 3 Load force of PET-R melt and nanocomposites filled with Cloisite 25A and additionally modified organoclays (the ''zero'' time is presented as the moment shortly after the start of mixing, when the values of load force can be measured).

0.01−100 rad/s, at the strains 2% for the nanocomposites, 30% for the matrix.

For an estimative investigation of viscosity during compounding, a load force generated by melt inside the mixing barrel was monitored.

Wide-angle X-ray scattering

The intensities of WAXS reflections were recorded at room temperature with a HZG 4/4A diffractometer (Praezisionsmechanik Freiburg, Germany). The Ni-filtered Cu Kα radiation generator was operated at 30 kV accelerating voltage and 30 mA current (wavelength $\lambda = 1.54$ Å). Patterns were recorded by monitoring those diffractions that appeared during angular scan from 1.4 to 10° (2θ) at a scanning rate of 1.5°/min.

Transmission electron microscopy

The TEM experiments were performed with a Zeiss LEO 912 Omega transmission electron microscope using an acceleration voltage of 120 keV. The samples were prepared using a Leica Ultracut UCT ultramicrotome equipped with a cryochamber. Thin sections of about 50 nm were cut with a Diatome diamond knife at −120°C.

Thermal characteristics

Thermal characterization of the polymer matrix and nanocomposites was carried out by differential scanning calorimetry (Pyris 1 DSC; Perkin Elmer, Waltham, MA) using a standard mode: (1) holding at 30°C for 3 min, (2) heating from 30 to 280°C at 10°C/min, (3) holding at 280°C for 2 min. The thermal parameters, glass transition temperature (T_g), cold crystallization temperature (T_c), melting temperature (T_m), enthalpy of cold crystallization (ΔH_c), and enthalpy of melting (ΔH_m) were calculated. The relative crystalline content (X_c) in nanocomposites was evaluated by assuming the ΔH_m for a hypothetical 100% crystalline PET to be 117.6 J/g.[47] Thermal stability of organoclays was tested using Perkin Elmer TGA 7 instrument equipped with a software Pyris 1. The samples were heated from 40 to 750°C at 10°C/min with a nitrogen purge of 20 mL/min.

Mechanical properties

For tensile tests an Instron 5800 R was employed. Experiments were measured according to ISO 527 and ISO 1873-2 standards. The crosshead speeds for tensile modulus measurements at 1 mm/min and for all other characteristics at 50 mm/min were adjusted.

RESULTS AND DISCUSSION

Melt rheology

Monitoring of viscosity during compounding

The load sensor of micro-extruder enables to monitor the downward force F_L that is generated by the pressure of transported melt. For a constant volume of the mixed material and constant processing speed, the F_L magnitude is proportional to the viscosity of the material. It is evident that all nanocomposite systems exhibit a decrease in F_L during mixing (Figs. 3–5) caused by degradation reactions.[46] However, the systems filled with organoclay modified with [3-(glycidyloxy)propyl]trimethoxysilane or hexadecyltrime-

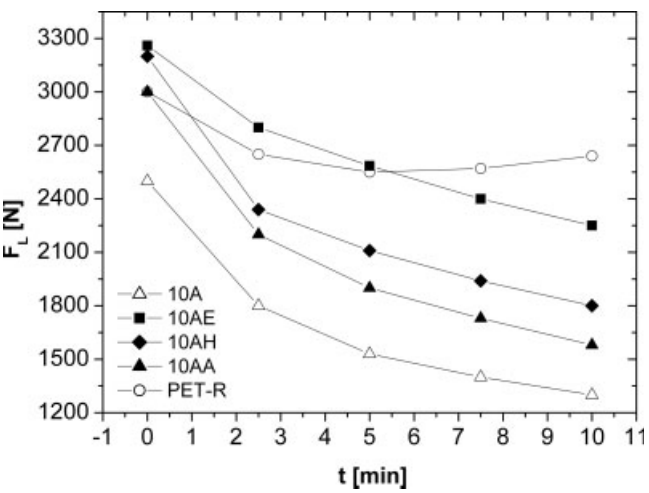

Figure 4 Load force of PET-R melt and nanocomposites filled with Cloisite 10A and additionally modified organoclays.

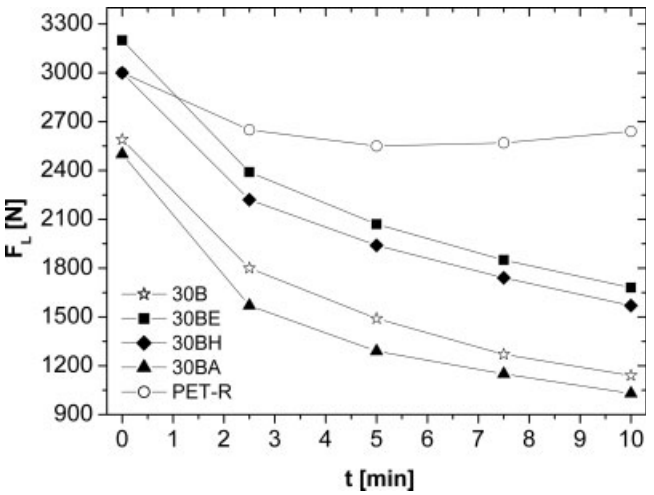

Figure 5 Load force of PET-R melt and nanocomposites filled with Cloisite 30B and additionally modified organoclays.

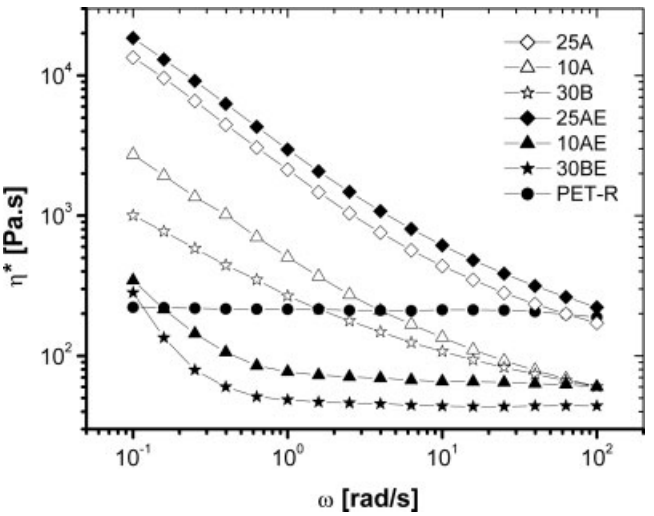

Figure 6 The complex viscosity versus frequency of the recycled PET matrix and nanocomposites.

thoxysilane show a significantly lower degradation tendency than the corresponding materials containing unmodified commercial nanofillers. Using the fillers C25AE, 10AE, and 30BE led to the lowest degradation (Figs. 3–5). Therefore, the effects of these modified organoclays on processing and utility properties of nanocomposites were compared with those of the best dispersed commercial nanofillers Cloisite 25A, 10A, and 30B.[46]

Complex rheological behavior

Dynamic shear flow properties of PET-R/organoclay nanocomposites were investigated in the region of linear viscoelasticity. The dynamic strain sweep test ($G'(\gamma)$) confirmed the linearity region in the range 1−100% strain for the matrix and 1−5% strain for the nanocomposites. According to our previous results, the color-selected recycled PET matrices and their blends exhibited a Newtonian behavior in the dependences $\eta^*(\omega)$ up to 100 rad/s and their complex viscosity decreased with increasing number of processing steps.[12]

In comparison with the matrix, complex viscosity of nanocomposites significantly increased in the range of low frequencies (more than 2 orders), as is shown in Figure 6. All the prepared nanocomposites show a shear thinning phenomenon, which is caused first by disruption of network structures and later on by orientation of filler particles in flow.

The results in Figure 6 demonstrate the highest filling effect of organoclay C 25AE. Moreover, the magnitude of complex viscosity of appropriate nanocomposite exceeded the value of matrix in the whole range of shear rates. That means significant reduction of degradation during the processing (visible also in Fig. 3). On the other hand, filling with C 10AE and 30BE exhibited adverse effect on viscosity (degradation tendency, described in Ref. 46). In this case, the complex viscosity decreased (comparing to systems with Cloisite 10A and 30B) together with very fast destruction of physical network (manifested itself by sharp viscosity decrease in the range of low shear rates). Generally, thermal stability of quaternary ammonium salts containing benzyl group[48] and resulting nanocomposites[49] is lower than that of systems with alkyl-based components. The several percentual decade mass loss of quaternary ammonium chlorides containing benzyl and long alkyl groups during the heating up to 200°C has been observed from TGA measurements due to cleavage of benzyl group.[50] The details dealing with

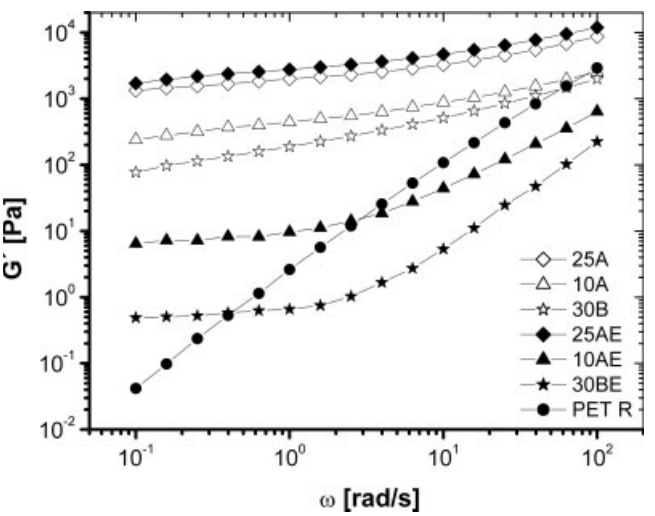

Figure 7 The storage modulus versus frequency of the recycled PET matrix and nanocomposites.

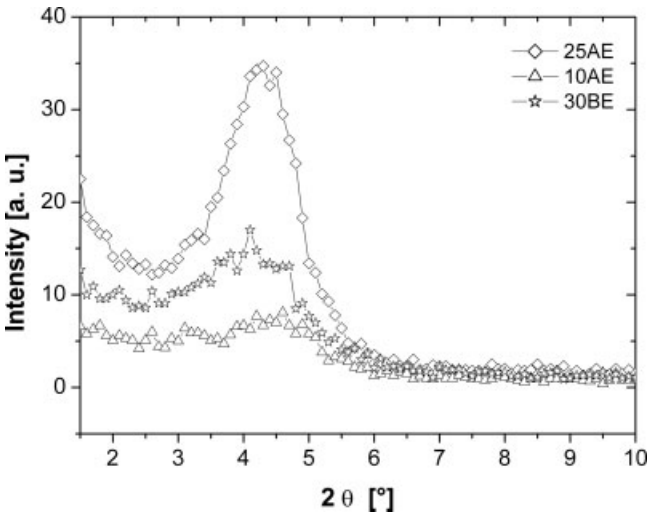

Figure 8 XRD patterns of pure fillers.

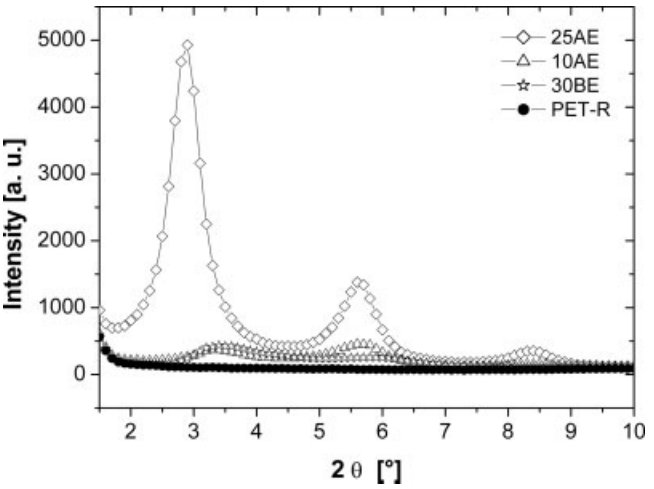

Figure 9 XRD patterns of matrix and nanocomposites.

adverse effect of Cloisite 30B on PET melt have been published in our previous work.[46]

The internal structural changes in nanocomposites during shear flow can be analyzed from frequency dependences of the storage (G') and loss (G'') moduli. Addition of clay to the PET-R melt causes an increase in the dynamic moduli, particularly in G' (Fig. 7). The pure matrix behaves as a viscoelastic liquid ($G'' > G'$). The higher value of G' than G'' for nanocomposites shows a change in viscoelastic behavior, i.e. a liquid-solid transformation. Moreover, the power-law dependence of the dynamic moduli at low frequencies, which is characteristic of the neat PET, is absent in the nanocomposites. The dependence of $G'(\omega)$ becomes nearly invariable. This ''secondary'' plateau indicates the formation of a network structure (exfoliation) of silicate layers in nanocomposites.[41,51,52]

An increase of G' in the mixture with C 25AE (comparing to system filled with Cloisite 25A and pure matrix) exhibits an enhancement of melt strength (Fig. 7). Nevertheless, an opposite effect of C 10AE and C 30BE fillers on elasticity in the melt state was observed as compared to Cloisite 10A and 30B. Therefore, the most remarkable G' ''secondary'' plateau was obtained in nanocomposites containing Cloisite 25A and C 25AE.

Morphology of organoclays in recycled PET

The prepared nanocomposites were analyzed by X-ray diffraction in the solid state to determine changes in the om-MMT interlayer distance caused by the insertion of PET between silicate layers. The effects of variations of their hydrophobicity and polar interactions on the structure in recycled PET were investigated and the results are shown in Figures 8 and 9. The influence of polymer intercalation on the arrangement of silicate layers is indicated by changes in the intensity, shape and peak positions of basal reflections. The basal spacings, d_{001}, were calculated from the observed peaks of the angular position 2θ according to Bragg's formula, $\lambda = 2d \sin \theta$. The level of intercalation is evaluated as Δd_{001}, which refer to the difference between the initial and final values of interlayer distance of organoclay (Table III).

TABLE III
XRD Analysis of Pure Organoclays and PET-R/Organoclay Nanocomposites

	XRD peak position (°)		Basal spacing (Å)		
Organoclay	Pure	Nanocomposite	Pure	Nanocomposite	Δd_{001} (Å)
Cloisite 25A	4.75[a]	3.1	18.6[a]	28.5	9.9
Cloisite 10A	4.6[a]	3	19.2[a]	29.4	10.2
Cloisite 30B	4.77[a]	2.9	18.5[a]	30.4	11.9
C 25AE	4.3	2.9	20.5	30.4	9.9
C 10AE	4.6	3.3	19.2	26.8	7.6
C 30BE	4.1	3.4	21.5	26	4.5

[a] Manufacturer's specification.

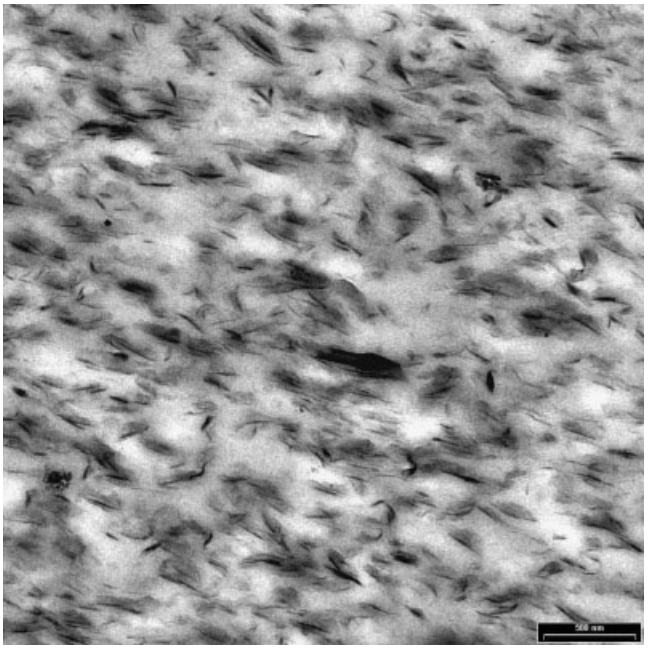

Figure 10 PET-R/Cloisite 25A (500 nm).

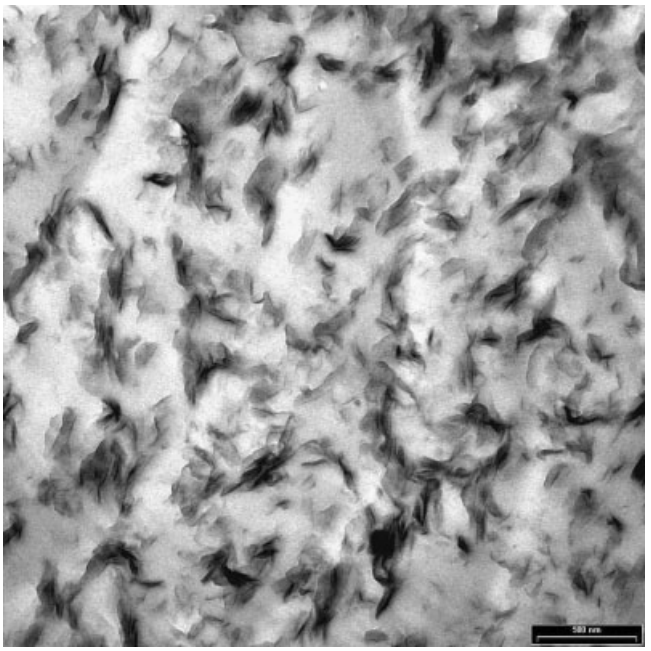

Figure 12 PET-R/Cloisite 25AE (500 nm).

The first peak of pure silanized organoclays C 25AE and C 30BE (Fig. 8, Table III) showed an increase of interlayer distance compared to Cloisite 25A and Cloisite 30B. Modification of Cloisite 10A resulted to equal intercalation (first peak at 4.6°). For the neat PET-R matrix the typical absence of peaks was found (Fig. 9). Concerning nanocomposite systems, silanization of Cloisite 25A led to similar increase of interlayer distance after melt mixing. The negative effect of C 30BE and C 10AE fillers (manifested itself by melt viscosity reduction, Fig. 6) exhibited also on significant decrease of Δd_{001} in appropriate nanocomposites (Table III).

The level of delamination/homogeneity is observable in TEM micrographs (Figs. 10–21) and is in good agreement with WAXS measurements. The systems filled with Cloisite 25A and C 25AE revealed similar partial exfoliation of silicate layers

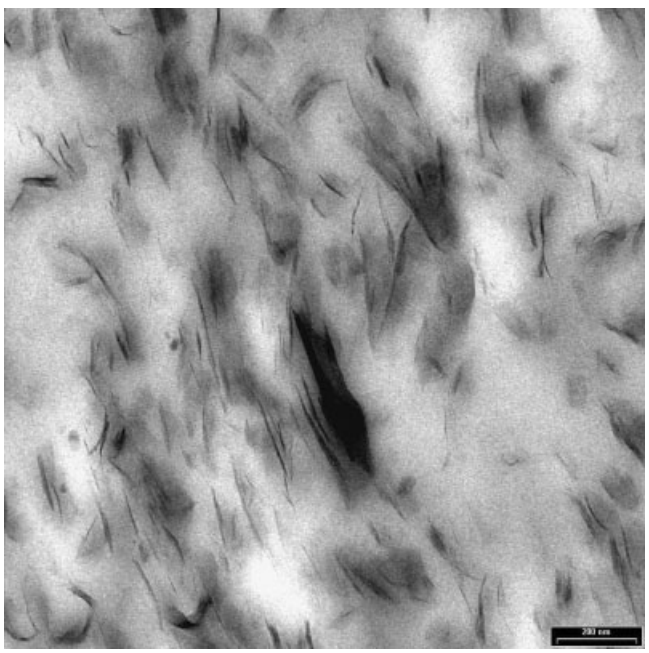

Figure 11 PET-R/Cloisite 25A (200 nm).

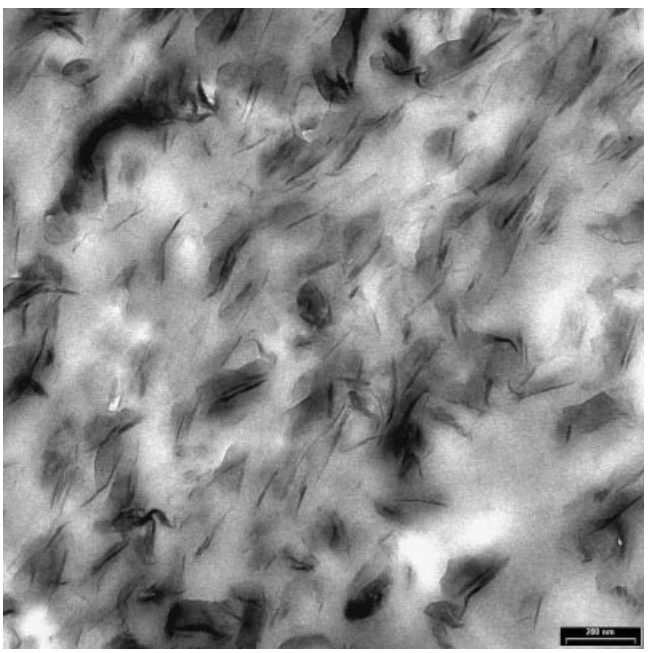

Figure 13 PET-R/Cloisite 25AE (200 nm).

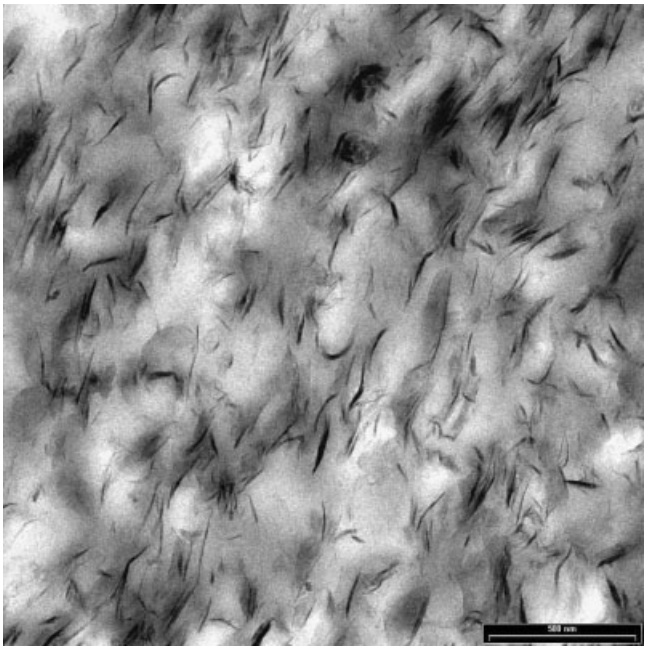

Figure 14 PET-R/Cloisite 10A (500 nm).

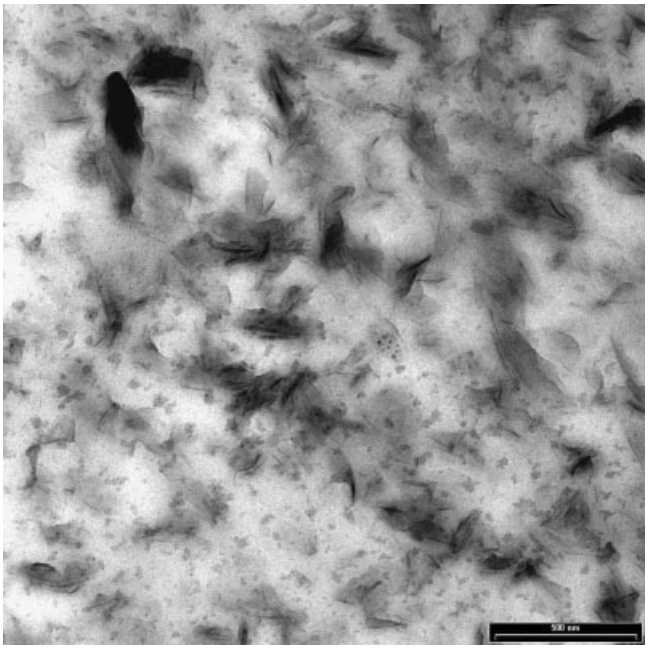

Figure 16 PET-R/Cloisite 10AE (500 nm).

(Figs. 10 and 12). From the 200-nm scale pictures (Figs. 11 and 13), a slightly higher homogeneity of nanocomposite containing C 25AE can be found. On the other hand, dispersion of C 30BE and C 10AE platelets in PET-R had a deteriorative impact on both exfoliation as well as homogeneity (Figs. 14–21). Pictures with resolution of 200 nm clearly show exfoliated structures as well as tactoids with lateral dimensions between 100 and 300 nm. Micrographs at the 500-nm scale show rather overall level of dispersion.

It is assumed that delamination decrease of C 30BE and C 10AE fillers in PET-R matrix arise from chemical reactions between the quaternary ammonium cations of commercial organoclays and [3-(glycidyloxy)propyl]trimethoxysilane. In the case of Cloisite 30B and Cloisite 10A, the organic modifiers are enabled to react directly with polymer chains and

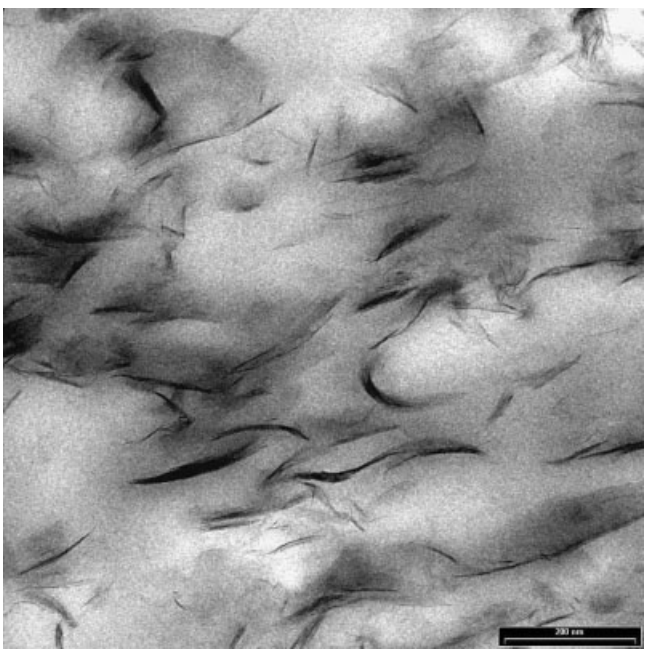

Figure 15 PET-R/Cloisite 10A (200 nm).

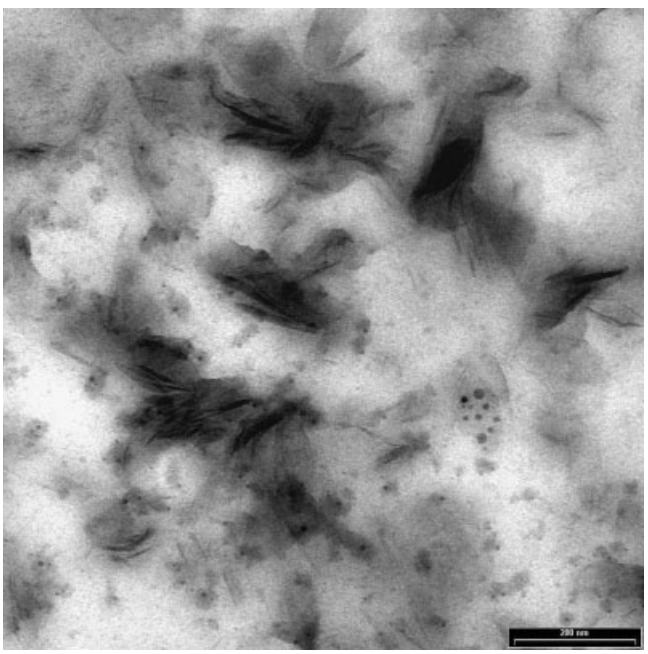

Figure 17 PET-R/Cloisite 10AE (200 nm).

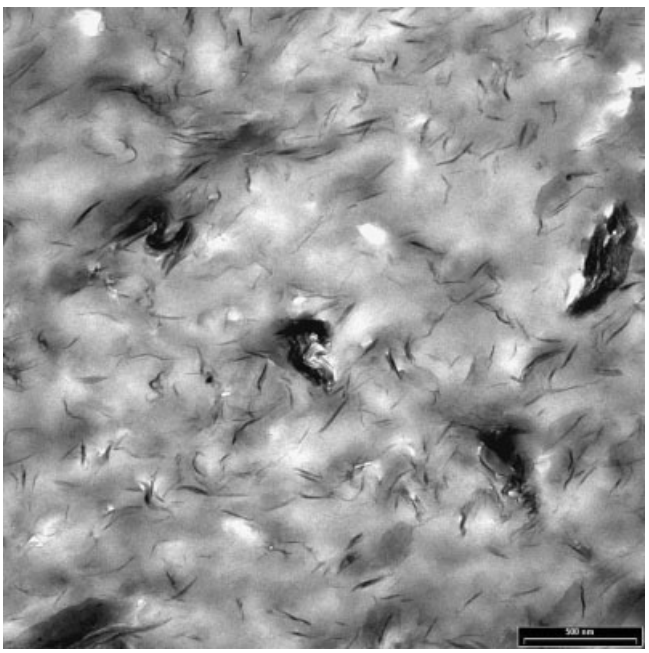

Figure 18 PET-R/Cloisite 30B (500 nm).

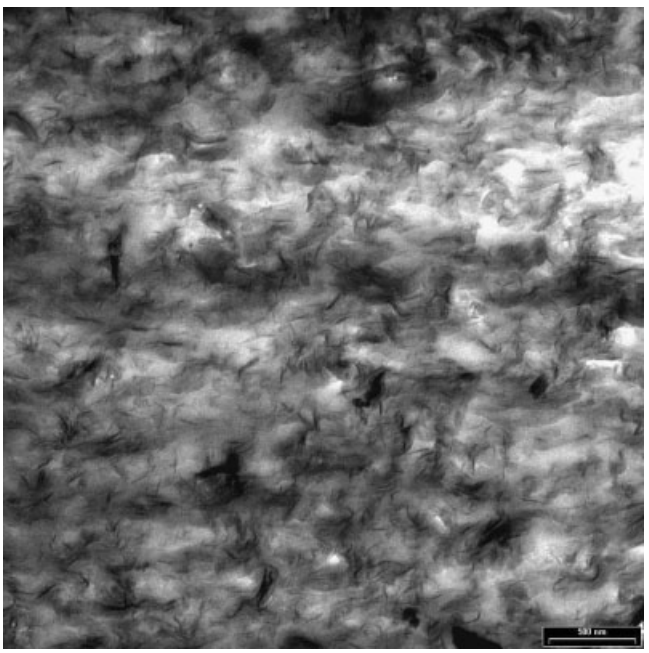

Figure 20 PET-R/Cloisite 30BE (500 nm).

thereby to facilitate increase of interlayer distance. This possibility of delamination in C 30BE and C 10AE silicates is considerably reduced by mechanism described.

Thermal characteristics

Thermal properties of nanocomposites were studied by DSC and TGA methods (Table IV). The systems filled with silanized organoclays (compared to composites containing commercial fillers) revealed decrease in total crystallinity and melting temperature together with faster formation of crystalline nuclei (decline in enthalpy of cold crystallization ΔH_c) during cooling in injection mould. In comparison with commercial organoclays, an effect on decrease in T_g and T_c temperature with C 25AE loading and opposite tendency with C 10AE and C 30BE usage was observed. This phenomenon can be explained as an increase of free volume (decrease of

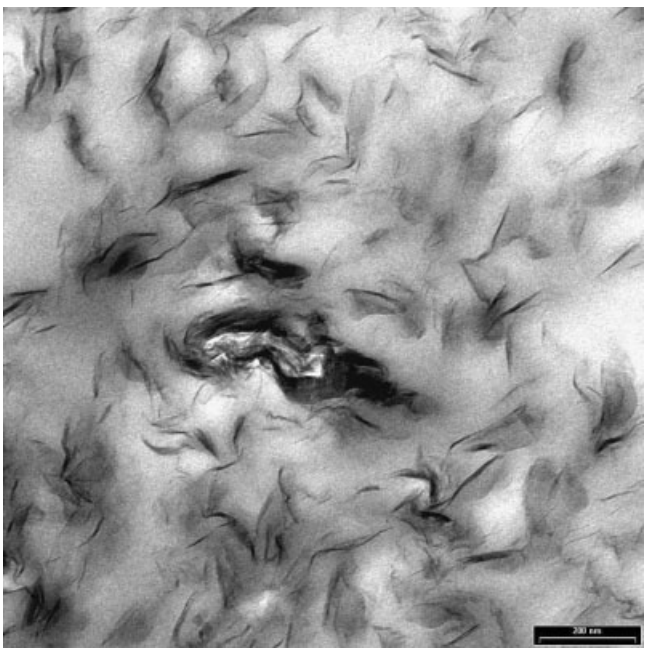

Figure 19 PET-R/Cloisite 30B (200 nm).

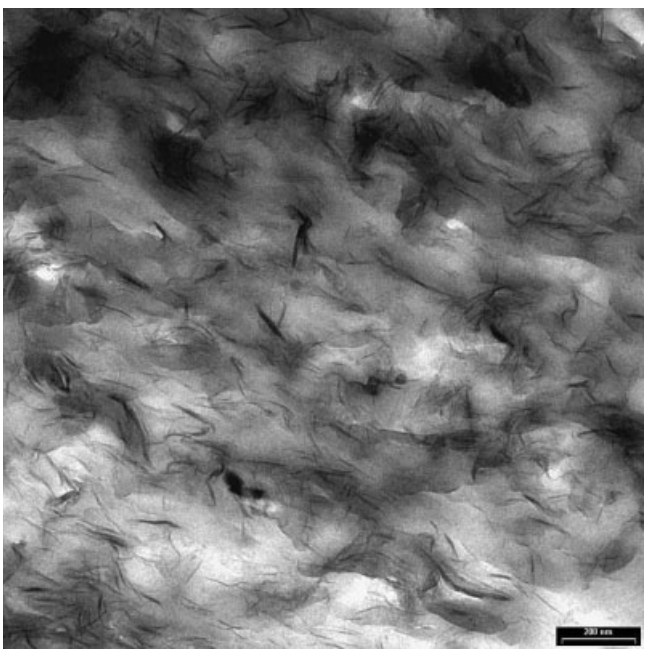

Figure 21 PET-R/Cloisite 30BE (200 nm).

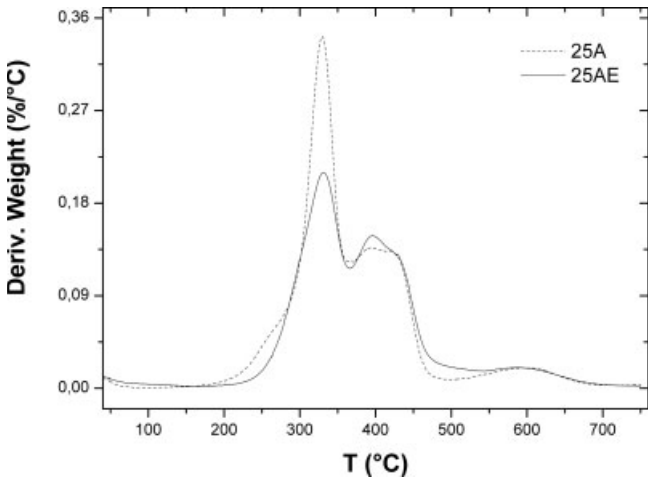

Figure 22 Thermogravimetric decomposition curves of Cloisite 25A and additionally modified organoclay.

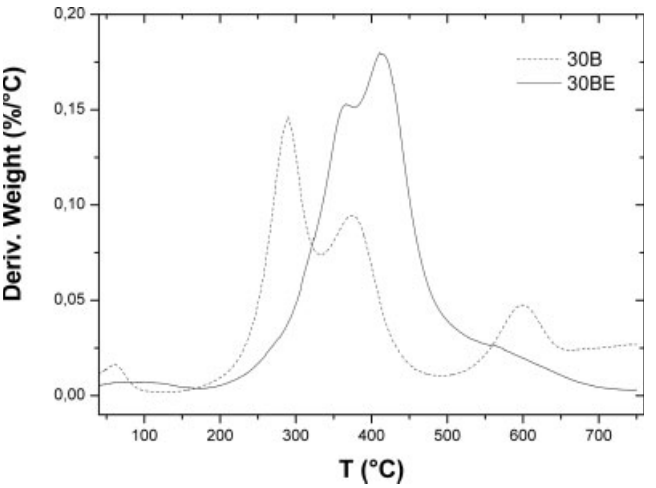

Figure 24 Thermogravimetric decomposition curves of Cloisite 30B and additionally modified organoclay.

T_g) with a higher delamination of silicate layers (Figs. 11 and 13). On the contrary, smaller surface area of tactoids causes weak interactions with polymer matrix resulting in decrease in free volume and increase in T_g (Figs. 15 vs. 17, 19 vs. 21). This relation is in accordance with WAXS and TEM analysis (Table III, Figs. 10–21). It is assumed that delaminated silicate platelets reduce mobility and consequently crystallization ability of polymer chains. This phenomenon is possible to observe as a crystallinity decline of nanocomposites compared to neat matrix, except the system with Cloisite 30B. The crystallinity growth in this composite implies that hydroxyl groups of Cloisite 30B modifier and the presence of undispersed silicate tactoids facilitate formation of crystalline nuclei.

The thermal stability of modified organoclays was increased, as evaluated in Figures 22–24 and Table V. Compared with commercial silicates, the significant enhancement was achieved in organoclays C 10AE and C 30BE, where the first decomposition peak was shifted from 242 to 319°C (Fig. 23) and from 290 to 366°C, respectively (Fig. 24). However, the strong effect of these organoclays on free water retention (evaporation peaks shifted approximately from 60 to 80°C) was observed. TGA patterns of Cloisite 25A and its silanized version were nearly unchanged.

The mass loss at 500°C was considerably decreased by silanization of Cloisite 10A and Cloisite 25A, while organoclay C 30BE exhibited opposite tendency. Nevertheless, all the modified versions of commercial clays manifested significant growth of temperature at both 5% as well as 10% mass loss (Table V).

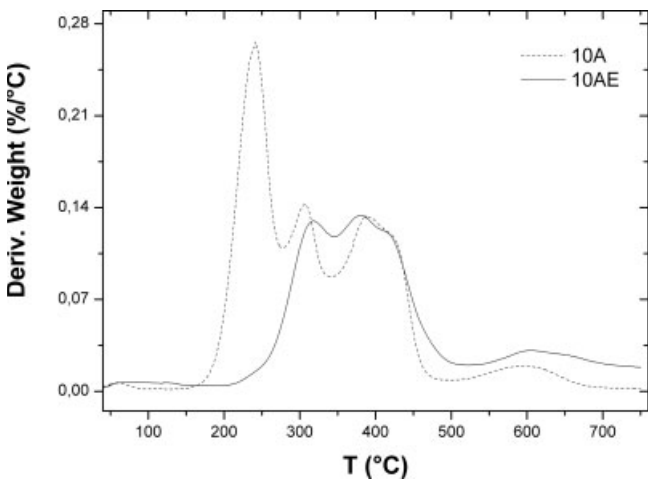

Figure 23 Thermogravimetric decomposition curves of Cloisite 10A and additionally modified organoclay.

TABLE IV
Thermal Properties of Nanocomposites and Neat Matrix

Sample	T_g[a] (°C)	T_c[b] (°C)	T_m[c] (°C)	ΔH_c[d] (J/g)	ΔH_m[e] (J/g)	X_c[f] (%)
PET-R/Cloisite 25A	72.6	122.3	254	25.3	41.4	35.2
PET-R/C 25AE	65.3	116.4	251.8	5.9	37.2	31.6
PET-R/Cloisite 10A	67.4	114.5	254.4	23.7	42.4	36.1
PET-R/C 10AE	75.6	118.8	250.8	13.5	38.3	32.6
PET-R/Cloisite 30B	72.8	118.1	254.6	25.5	46	39.1
PET-R/C 30BE	78.2	121.9	251.9	17.3	40.6	34.5
PET-R	75.6	123.2	252.2	24.9	43.2	36.7

[a] Glass transition temperature.
[b] Cold crystallization temperature.
[c] Melting point.
[d] Enthalpy of cold crystallization.
[e] Enthalpy of melting.
[f] Relative crystalline content.

Tensile characteristics

The mechanical properties of PET-R and appropriate nanocomposites are listed in Table VI. The systems containing fillers C 10AE and C 30BE were not measured due to their deteriorative effect on rheological properties (Figs. 6 and 7). In comparison to recycled polymer, the stiffness of all the composite systems was substantially increased. On the contrary, the tensile strength and extensibility were decreased. However, nanocomposite filled with C 25AE revealed interesting combination of high stiffness and satisfactory level of extensibility. The large elongation of PET-R/25AE nanocomposite results from high interfacial adhesion (increased polarity of Cloisite 25A by modification with [3-(glycidyloxy)-propyl]trimethoxysilane match more the polar feature of PET) and from the lowest degradation (compared to other systems filled with silanized organoclays) during the processing (proved in Fig. 6).

CONCLUSIONS

Recycled PET/organoclay nanocomposites were prepared by a melt intercalation method. According morphological analysis, C 25AE (from the group of modified organoclays) and Cloisite 25A (from the group of commercial fillers) were shown to be the most dispersed organoclays in the recycled PET matrix. The highest level of intercalation Δd_{001} was obtained using the filler Cloisite 30B. However, some bigger stacks of these clay platelets were found in TEM micrographs. Rheological study showed the complex flow behavior of the nanocomposites and melt behavior during compounding. The significant increase in the complex viscosity and storage modulus with organoclay loading was observed at low frequencies, where the viscoelastic liquid of recycled PET changed into nanocomposites with a solid-like behavior. The filling with C 25AE exhibited enhancing effect on rheological properties of nanocomposite. On the other hand, silanization of Cloisite 10A and 30B led to significant loss of melt strength, which is attributed to higher water retention of silicates together with chemical reactions between the organic groups of organoclays and [3-(glycidyloxy)-propyl]trimethoxysilane modifier. The moderate ''secondary'' plateau on the G' frequency dependence confirmed the network formation in the nanocomposites, qualitatively explained by polymer–filler and particle–particle interactions. A correlation between commercial and silanized organoclays effect on linear viscoelastic flow characteristics and dispersion level (TEM and WAXS) of the prepared nanocomposites was found. Thermal characterization of nanocomposites filled with additionally modified organoclays compared with that of containing commercial organoclays revealed reduction of crystalline content and melt temperature together with higher crystallization rate during injection molding. The change of glass transition and cold crystallization temperature depending on delamination level was observed. Thermal stability of commercial organoclays was enhanced by silanization. The mechanical testing confirmed growth of stiffness up to 38% with organoclay loading and for system containing C 25AE also sufficient extensibility was reached. This property can be interesting for applications in fiber and film industry (combination of high stiffness with extensibility).

TABLE V
Thermogravimetric Decomposition Characteristics of Organoclays

Organoclay	5% Mass loss (°C)	10% Mass loss (°C)	500°C mass loss (%)
Cloisite 30B	279.1	324.2	17.7
Cloisite 30BE	327.2	366.1	25
Cloisite 25A	298.5	321.0	30.6
Cloisite 25AE	304.6	331.3	27
Cloisite 10A	224.6	244.1	34.3
Cloisite 10AE	303.6	343.6	23.3

TABLE VI
Mechanical Properties of the Neat Matrix and Nanocomposites

Sample	Tensile modulus (MPa)	Tensile strength (MPa)	Elongation at break (%)
PET-R	2170	57.1	316.5
PET-R/Cloisite 30B	2905	42.3	5.1
PET-R/Cloisite 10A	2523	33.7	19.2
PET-R/Cloisite 25A	2984	26.6	30.6
PET-R/C 25AE	2810	22	244.6

The authors gratefully appreciate the work of Dr. Jana Kovářová (TGA measurements) and Dr. Josef Baldrian (WAXS measurements) from Institute of Macromolecular Chemistry.

References

1. Rwei, S. P. Polym Eng Sci 1999, 39, 12.
2. Wang, C. S.; Sun, Y. M. J Polym Sci Part A: Polym Chem 1994, 32, 1295.
3. Stewart, M. E.; Cox, A. J.; Naylor, D. M. Polymer 1993, 34, 4060.
4. Gargiulo, C.; Belletti, G. Chem Fibres Int 1997, 47, 28.
5. PETCORE Association (PET Containers Recycling Europe), http//www.petcore.org.
6. Kráčalík, M.; Pospíšil, L.; Šimoník, J.; Kimmer, J.; Hrnčiřík, J. Plasty Kauc 2003, 40, 356.
7. Paszun, D.; Spychaj, T. Ind Eng Chem Res 1997, 36, 1373.
8. Mankosa, M. J.; Carver, R.; Venkatraman, P. Miner Eng 1997, 49, 46.
9. Lin, C. C. Macromol Symp 1998, 135, 129.

10. Koester, E. Mater World 1997, 9, 525.
11. Pegoretti, A.; Kolarik, J.; Peroni, C.; Migliaresi, C. Polymer 2004, 45, 2751.
12. Kráčalík, M.; Hrnčiřík, J.; Pospíšil, L.; Šimoník, J. In Proceedings of PPS-18 International Conference, Guimaraes, Portugal, June 16–20, 2002, p 139.
13. Lee, K. M.; Han, C. D. Macromolecules 2003, 36, 7165.
14. Ray, S. S.; Okamoto, M. Prog Polym Sci 2003, 28, 1539.
15. Olphen, H. Clay Colloid Chemistry; Wiley: New York, 1977.
16. Lee, J. F.; Mortland, M. M.; Chiou, C. T.; Kile, D. E.; Boyd, S. A. Clays Clay Miner 1990, 38, 113.
17. Gilman, J. W.; Morgan, A. B.; Harris, R. H., Jr.; Trulove, P. C.; DeLong, H. C.; Sutto, T. E. Polym Mater Sci Eng 2000, 83, 59.
18. Imai, Y.; Nishimura, S.; Abe, E.; Tateyama, H.; Abiko, A.; Yamaguchi, A.; Aoyama, T.; Taguchi, H. Chem Mater 2002, 14, 477.
19. Maxfield, M.; Shacklette, L. W.; Baughman, R. H.; Christiani, B. R.; Eberly, D. E. Int. Pat. WO 93/04118 (1993).
20. Lee, S. S.; Kim, J. Polym Mater Sci Eng 2003, 89, 370.
21. Takekoshi, T.; Khouri, F. F.; Campbell, J. R.; Jordan, T. C.; Dai, K. H. U.S. Pat. 5,530,052 (1996).
22. Ke, Y. C.; Long, C.; Qi, Z. J Appl Polym Sci 1999, 71, 1139.
23. Sekelik, D. J.; Stepanov, E. S.; Schiraldi, D.; Hiltner, A.; Baer, E. J Polym Sci Part B: Polym Phys 1999, 37, 847.
24. Matayabas, J. C., Jr.; Turner, S. R.; Sublett, B. J.; Connell, G. W.; Barbee, R. B. Int. Pat. WO 98/29499 (1998).
25. Pinnavaia, T. J.; Beall, G. W. Polymer–Clay Nanocomposites; Wiley: Chichester, 2000.
26. Imai, Y.; Inukai, Y.; Tateyama, H. Polym J 2003, 35, 230.
27. Barber, G. D.; Moore, R. B. Abstr Pap Am Chem Soc 2000, 219, 131-PMSE Part 2, 241.
28. Ou, C. F.; Ho, M. T.; Lin, J. R. J Polym Res 2003, 10, 127.
29. Davis, C. H.; Mathias, L. J.; Gilman, J. W.; Schiraldi, D. A.; Shields, J. R.; Trulove, P.; Sutto, T. E.; Delong, H. C. J Polym Sci Part B: Polym Phys 2002, 40, 2661.
30. Sanchez-Solis, A.; Garcia-Rejon, A.; Manero, O. Macromol Symp 2003, 192, 281.
31. Sanchez-Solis, A.; Romero-Ibarra, I.; Estrada, M. R.; Calderas, F.; Manero, O. Polym Eng Sci 2004, 44, 1094.
32. Hoffmann, B.; Dietrich, C.; Thomann, R.; Friedrich, C.; Mülhaupt, R. Macromol Rapid Commun 2000, 21, 57.
33. Hoffmann, B.; Kressler, J.; Stöppelmann, G.; Friedrich, C.; Kim, G. M. Colloid Polym Sci 2000, 278, 629.
34. Solomon, M. J.; Almusallam, A. S.; Seefeldt, K. F.; Somwangthanaroj, A.; Varadan, P. Macromolecules 2001, 34, 1864.
35. Hyun, Y. H.; Lim, S. T.; Choi, H. J.; Jhon, M. S. Macromolecules 2001, 34, 8084.
36. Ray, S. S.; Yamada, K.; Okamoto, M.; Ueda, K. Polymer 2003, 44, 857.
37. Incarnato, L.; Scarfato, P.; Scatteia, L.; Acierno, D. Polymer 2004, 45, 3487.
38. Lepoittevin, B.; Devalckenaere, M.; Pantoustier, N.; Alexandre, M.; Kubies, D.; Calberg, C.; Jérôme, R.; Dubois, P. Polymer 2002, 43, 4017.
39. Lee, K. M.; Han, C. D. Polymer 2003, 44, 4573.
40. Kotsilkova, R. Mech Time-Dependent Mater 2002, 6, 283.
41. Krishnamoorti, R.; Giannelis, E. P. Macromolecules 1997, 30, 4097.
42. Kim, T. H.; Jang, L. W.; Lee, D. C.; Choi, H. J.; Jhon, M. W. Macromol Rapid Commun 2002, 23, 191.
43. Gelfer, M.; Song, H. H.; Liu, L.; Avila-Orta, C.; Yang, L.; Si, M.; Hsiao, B. S.; Chu, B.; Rafailovich, M.; Tsou, A. H. Polym Eng Sci 2002, 42, 1841.
44. Wagener, R.; Reisinger, T. J. G. Polymer 2003, 44, 7513.
45. Lim, S. T.; Hyun, Y. H.; Choi, H. J.; Jhon, M. S. Polym Prepr 2001, 42, 640.
46. Kráčalík, M.; Mikešová, J.; Puffr, R.; Baldrian, J.; Thomann, R.; Friedrich, C. Polym Bull 2007, 58, 313.
47. Metha, A.; Wunderlich, B. J Polym Sci Polym Phys Ed 1978, 16, 289.
48. Busi, S.; Lahtinen, M.; Kaernae, M.; Valkonen, J.; Kolehmainen, E.; Rissanen, K. J Mol Struct 2006, 787, 18.
49. Su, S.; Jiang, D. D.; Wilkie, Ch. A. Polym Degrad Stab 2004, 84, 269.
50. Avram, E. Rev Romaine de Chim 2001, 46, 49.
51. Khan, S. A.; Prud'homme, R. K. Rev Chem Eng 1987, 4, 205.
52. Krishnamoorti, R.; Vaia, R. A.; Giannelis, E. P. Chem Mater 1996, 8, 1728.